# Thermo-mechanical Behavior Analysis of Multipurpose Research Reactor Fuel Assembly Using Fluid–Structure Interaction (FSI) with ANSYS Workbench: Comparative Validation Between Fluent and CFX

SHAH NUSRAT JAHAN SHANTA, NUSRAT ZAHAN ZARIN,
ABDUS SATTAR MOLLAH*
Department of Nuclear Science and Engineering, Military Institute of Science and Technology,
Mirpur Cantonment, Dhaka,
BANGLADESH
**Corresponding author*

*Abstract:* - Bangladesh desires to upgrade its nuclear research capacity by commissioning a 10–20 MW multi-purpose research reactor (MPRR) to be fueled by VVR-KN low-enriched uranium (LEU) fuel in terms of the limitation of its current 3 MW TRIGA Mark-II reactor, specifically in fuel supply issues. In this study, the fuel assembly is solved by applying a fluid–structure interaction (FSI) approach in ANSYS Workbench to analyze coupled thermal, hydraulic and structural responses under steady-state operating conditions. The solution integrates computational fluid dynamics (CFD) with structural mechanics to analyze coolant flow behavior, temperature distribution, pressure drop, energy gains and resulting fuel rod deformations, stress, strain. Comparative analysis is carried out between ANSYS Fluent and ANSYS CFX solvers to verify consistency and accuracy of results. Comparative validation confirms the robustness of FSI framework that accurately predicts thermo-mechanical safety margins of MPRR safety assembly.

*Keywords: MPRR, VVR-KN, FSI, CFX, k–ϵ.*

Received: April 23, 2025. Revised: July 15, 2025. Accepted: August 14, 2025. Published: January 28, 2026.

## 1. Introduction

Research reactors are essential instruments used for scientific research, training, and radioisotope production for various purposes such as materials science, medicine, neutron science, radioisotope production, materials testing, and nuclear physics, etc. In power reactors, these facilities are operated at very low power levels (typically below 20 MW) and are designed mainly for neutron production and not electricity production [1].

Bangladesh has been expanding its nuclear research activities utilizing the 3 MW TRIGA Mark-II research reactor that has been operating since 1986 at the Atomic Energy Research Establishment, Savar. The Bangladesh Atomic Energy Commission (BAEC)-operated reactor has been utilized in various applications, including neutron activation analysis, neutron radiography, neutron scattering, radioisotope production (for instance, Iodine-131 and Technetium-99m), and manpower training [2]. Nevertheless, the viability of this facility is questioned by limited supplies of its particular fuel type, uranium-zirconium hydride, which, though restarted by TRIGA International since 2021, continues to be limited by modest worldwide production and the absence of a guaranteed fuel supply agreement for Bangladesh [3]. Bangladesh is going to acquire a higher capacity multi-purpose research reactor (MPRR) of 10-20 MW power with VVR-KN low-enriched uranium (LEU) fuel. This low-enriched uranium fuel is used into VVR-K reactor which is relatively affordable and easy-going [4].

The temperature gradient across the fuel assembly thickness, which is time-dependent under different operating transients, is evaluated as part of thermo-mechanical analysis [12]. The temperature profile has some impact on the fuel elements' mechanical performance. Therefore, it is essential to carry out the thermal-mechanical analysis while taking fuel element burnup effects into account [13]. Structural analysis is required to recognize the mechanical behavior of the fuel under normal operating conditions and identify potential problems [5]. To ensure safety and reliability, to calculate thermal loads and nuclear system mechanical stresses, research reactors offer the controlled environment necessary to experimentally test and validate the thermo-mechanical properties of fuel assemblies.

In addition, research into the thermo‑mechanical behavior of reactor fuel assemblies has attained a high level of importance due to its direct relation with reactor safety, operational reliability, and structural integrity. New opportunities are created by state-of-the-art numerical methods such as Fluid–Structure Interaction for analyzing the coupled behavior of coolant flow and structural deformation in a more accurate way. FSI (Fluid–Structure Interaction) is the interaction between a rigid or flexible structure and an interior or adjacent fluid flow [6]. This work proposes an interface control principle for unsteady fluid-structure interaction analyses. The principle provides a means to explicitly control the interface motion in the temporal direction in such a way as to minimize the residual force on the interface, defined as the discrepancy between the fluid and structural forces [11]. The fluid

applies pressure, temperature, and vibrational forces to the structure and the structure deforms under these forces, and this in turn modifies the fluid flow pattern. FSI is required to achieve the coupled behavior of fuel structure and coolant flow, ensuring both performance and safety of the reactor fuel assembly.

## 2. Methodology

The thermo-mechanical study of MPRR fuel assembly is carried out using coupled FSI method within ANSYS which designed to capture the mutual dependence between fluid flow, heat transfer, and structural deformation, the time stepping iterative data converging is achieved and the flowchart of the simulation method is represented in Fig 1 [7].

The simulation starts with geometry construction of the fuel assembly where the parameters of fuel and coolant regions are defined. The geometry module provides separate domains for fluid and solid regions to permit an understandable definition of the FSI boundary. The Fluent/CFX solver module controls the CFD analysis by determining velocity, pressure, and temperature distributions in the coolant, where the Mechanical solver module resolves thermal stress and deformation in the fuel plates. Figure 2 shows the working module of the FSI (Fluent) model. 3D geometry is created by using ANSYS Design Modeler which is shown in Fig 3.

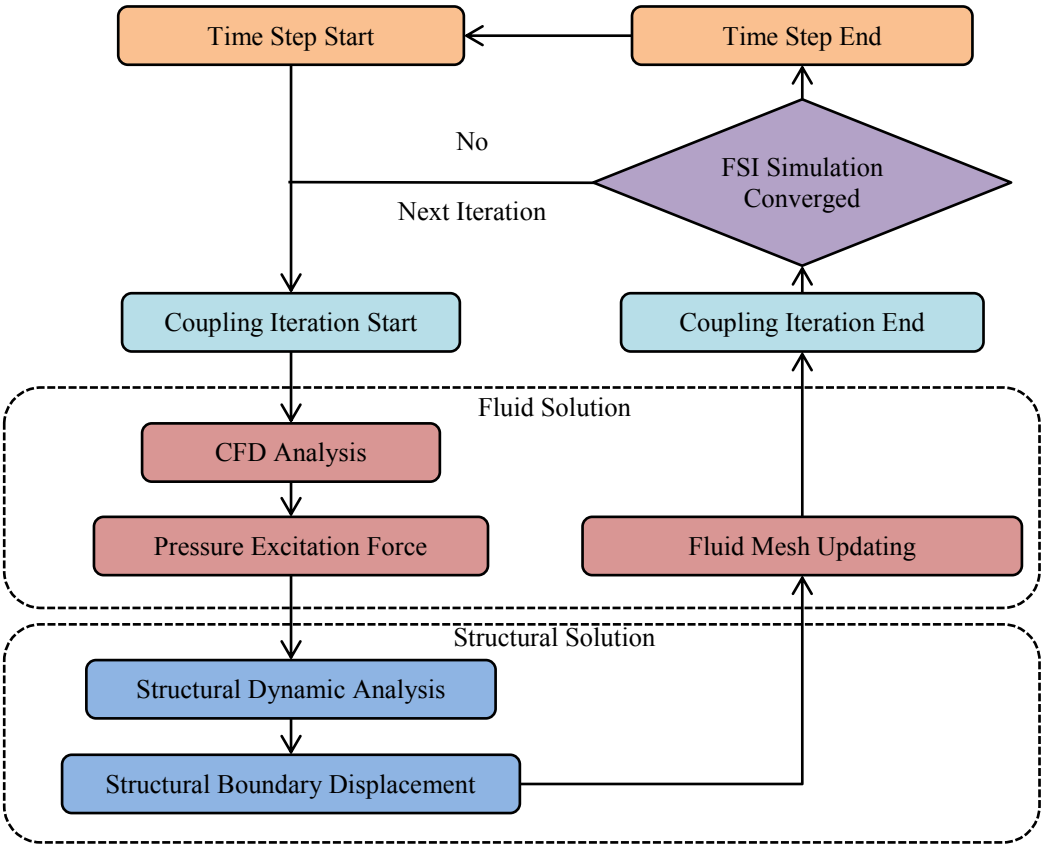


Figure 1. Flow chart of FSI method.

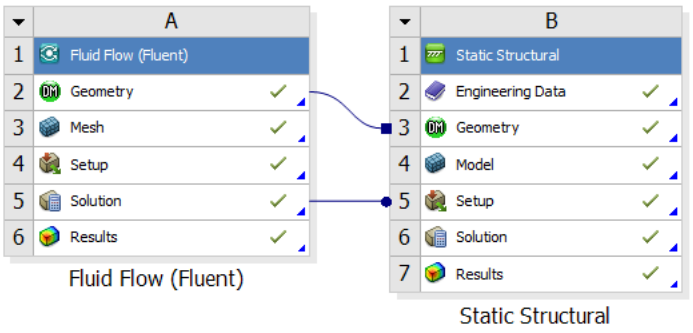


Figure 2. Working module of FSI model.

The two-way FSI simulation was performed using an iterative coupling procedure in ANSYS Workbench, where separate fluid and structural solvers exchange information at their interface within each time step until convergence is achieved. The CFD solver first calculated pressure, temperature, and shear loads on the fuel plates, which were transferred to the structural solver to compute deformation, stress, and strain. The updated displacements were then fed back to the CFD solver to update the fluid mesh and recalculate the flow field. This fluid–solid data exchange continued until all convergence criteria were met. For the CFD domain, residuals for continuity, momentum, and energy equations were required to fall below $10^{-5}$, with mass imbalance under 0.1%. For the structural domain, the relative change in displacement and equivalent stress between successive iterations had to fall below $1 \times 10^{-4}$. Coupling convergence was achieved when interface force and displacement changes were less than 1%, after which the solution proceeded to the next time step.

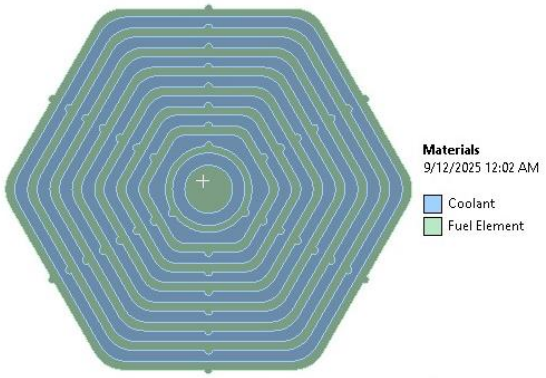


Figure 3. Designed geometry of MPRR fuel assembly.

A high-resolution mesh is generated for both fluid turbulence and solid domains. Fluid domain is meshed by using a hybrid meshing method, with hexahedral elements in the bulk flow regime to ensure numerical stability and inflation layers near fuel plate walls to accurately capture boundary layer effects. For structural domain, meshed by using quadratic tetrahedral elements to capture stress gradients. The meshing result of the fuel assembly is mentioned in Fig 4.

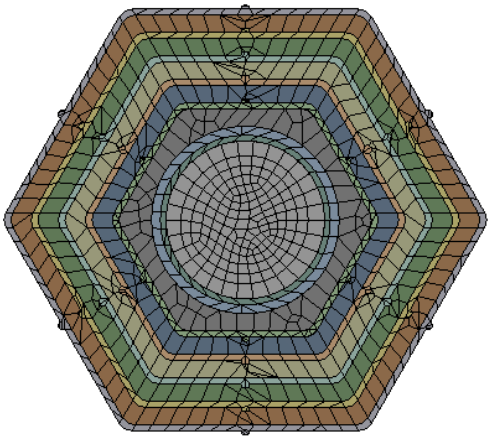

Figure 4. Pictorial View Meshing.

The mesh convergence study shows in fig 5. and table 1 which is performed using six different mesh configurations, including adaptive, 2 mm, 2.5 mm, 3 mm, 3.4 mm, and 4 mm element sizes, to investigate the effect of mesh refinement on the solution accuracy. The results reveal that while adaptive and very fine meshes slightly improve accuracy, the variation in total deformation, equivalent stress, strain, and strain energy becomes minimal beyond the 3 mm mesh size, indicating that the solution has reached mesh independence. Such as, the total deformation for 3 mm and 3.4 mm meshes differs by only 0.45%, and the equivalent stress varies by less than 0.2%, which is negligible from an engineering perspective. Additionally, the skewness values across all meshes remain within the acceptable range, ensuring good element quality. Considering the trade-off between computational cost and result accuracy, the 3 mm mesh size was selected for all subsequent analyses, as it offers sufficiently converged results with optimized computational efficiency.

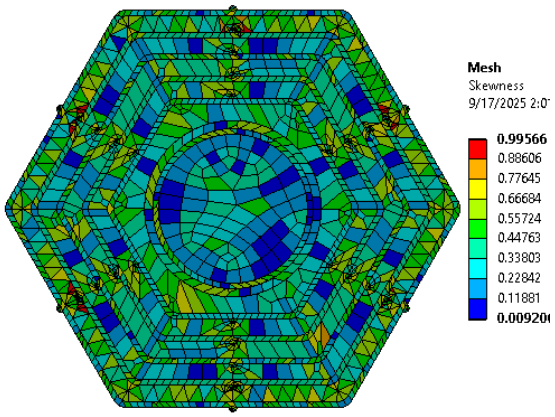


(a) Mesh Size -adoptive

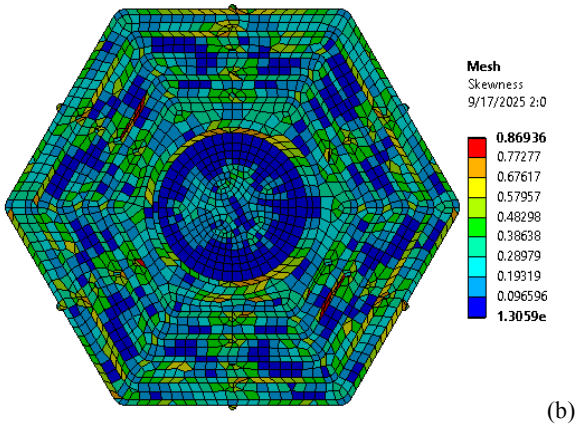


(b)

Mesh Size -. 2 mm

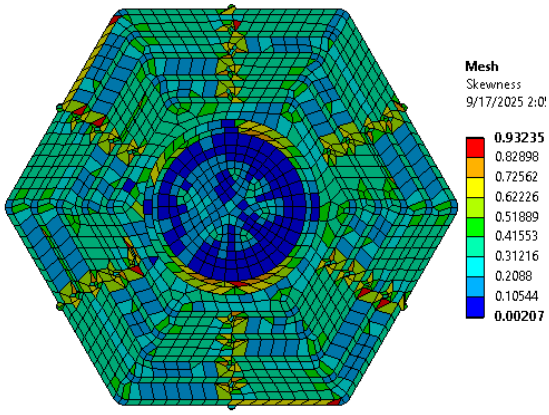


(c) Mesh Size - 2.5 mm

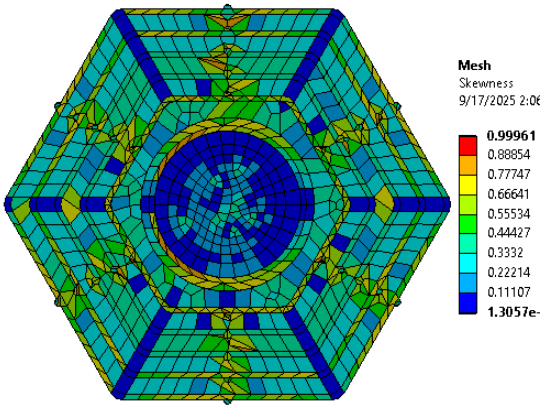


(d) Mesh Size - 3 mm

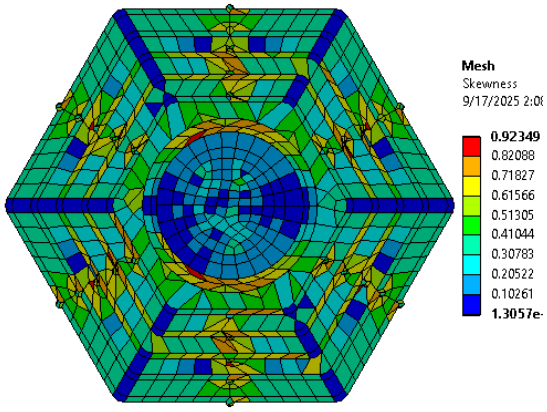


(e) Mesh Size - 3.4 mm

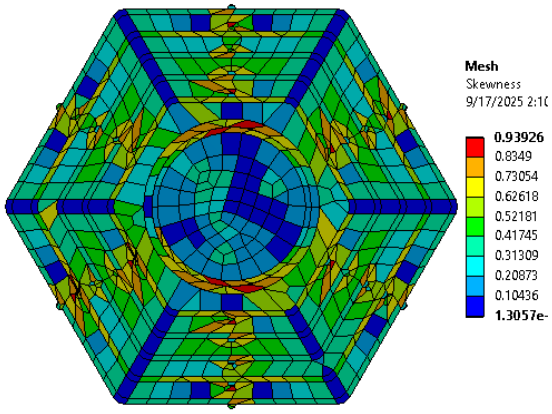


(f) Mesh Size - 4 mm

Figure 5. Display of the color contour of skewness for different mesh size

Table 1. Mesh Convergence Table

| **Mesh size** | **Skewness** $\times 10^{-2}$ | **Deformation** $\times 10^{-3}$, **µm** | **Stress,** $\times 10^{-2}$, **MPa** | **Strain,** $\times 10^{-7}$ | **Strain Energy** $\times 10^{2}$, **pJ** |
|---|---|---|---|---|---|
| adoptive | 51.126 | 29.832 | 44.552 | 22.353 | 67.62 |
| 2 mm | 34.209 | 31.026 | 48.775 | 24.411 | 16.52 |
| 2.5 mm | 38.636 | 30.423 | 54.888 | 27.444 | 22.79 |
| 3 mm | 43.41 | 30.1516 | 46.545 | 23.27 | 29.40 |
| 3.4 mm | 44.5 | 30.331 | 58.757 | 28.378 | 51.31 |
| 4 mm | 50.124 | 30.566 | 56.531 | 28.265 | 56.56 |

**N.B.** µm = micro meter; MPa = Mega Pascal; pJ = Picojoule; and skewness and strain are unit less

Table 2. Skewness and Mesh Quality List [10]

| Value of Skewness | 1 | 0.75 - 0.9 | 0.5 - 0.75 | 0.25 - 0.5 | >0 - 0.25 | 0 |
|---|---|---|---|---|---|---|
| Cell Quality | Degenerate | Poor | Fair | Good | Excellent | Equilateral |

Table 1 represents the effect of various mesh sizes on the thermo-mechanical outputs of the MPRR fuel assembly simulation with considered parameters. The result converges for 3 mm mesh size, after that the result diverges. So, 3mm mesh size is considered for further simulation. Table 2 shows the standard relationship between mesh skewness and cell quality, which is widely applied in computational fluid dynamics (CFD) for assessment of mesh accuracy and stability [10] and table 3 shows the tabular representation of mesh statistics for 3 mm mesh size. a skewness value of 0 represents an ideal equilateral cell, while values close to 1 indicate highly distorted or degenerate cells. When compared with the mesh sensitivity study (Table 1.), the 3mm mesh had a skewness value of 0.4341, which falls into "Good" range according to the table 2., indicating acceptable quality for accurate CFD and FSI simulations. Figure 6. shows the graphical depiction of mesh convergence test from the above data.

Table 3. Tabular Representation of Mesh Statistics For 3 Mm Mesh Size

| Parameters | Nodes | Elements |
|---|---|---|
| CFD Analysis | 3651453 | 2707593 |
| Structural Alalysis | 744065 | 119682 |

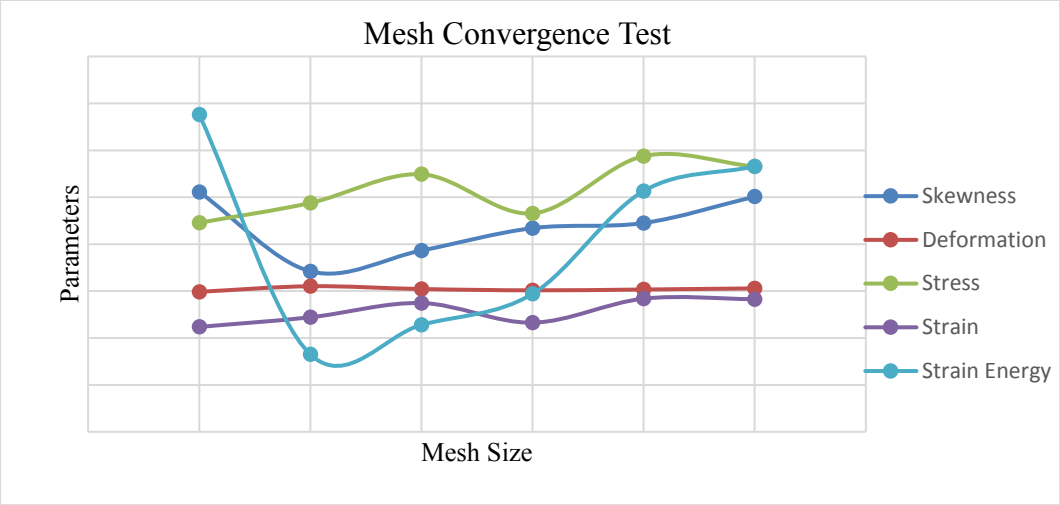


Figure 6. Graphical Representation of Mesh Convergence Test.

# 3. Governing Equations of the Coupled Simulation

## 3.1 Energy equation for CFD analysis,

$$\frac{d(\rho E)}{dt} + \nabla(\rho u E) = \nabla(k \nabla T) + \Phi \qquad (1)$$

Where,

ρ = fluid density;

E = total energy per unit volume, which is equal to internal energy plus kinetic energy;

t = time;

u = velocity vector;

k = thermal conductivity;

T = temperature;

$\nabla$ = gradient operator; and

Φ = source or sink terms that describe energy transfer owing to chemical reactions and heat transfer by conduction, convection, and radiation [8].

## 3.2 The Standard k–ε Model Equations

This model is used for turbulence flow. Equation 2 and 3 represent the mathematical expression of the k–ε model where equation 2 is used for k and equation 3 is used for ε.

$$\frac{d(\rho k)}{dt} + \nabla(\rho k U) = P - \varepsilon \qquad (2)$$

$$\frac{d(\rho \varepsilon)}{dt} + \nabla(\rho \varepsilon U) = C\mu\,(P - \varepsilon) \qquad (3)$$

Where,

ρ = fluid density;

t = time;

U = velocity vector;

P = turbulence production;

ε = turbulence dissipation rate;

Cμ = model constant; and

$\nabla$ = divergence operator [9].

We assumed the inlet velocity 12.26 m/s, inlet temperature of cladding is 356 K, and pressure is 0.135 MPa. The coupled simulation proceeds in discrete time steps which meet the convergence criteria and the iterative result is mentioned in Fig 8. And the location of the boundary for static structure is depicted in Fig 7.

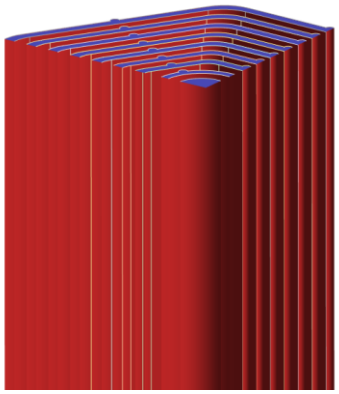


Figure 7. Boundary locations for structural analysis.

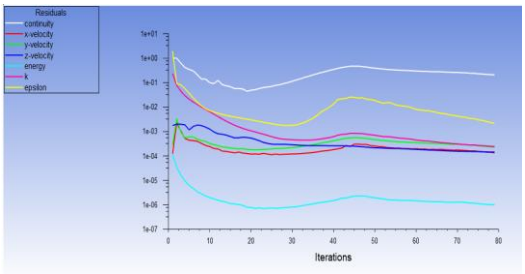


Figure 8. Iterative Solution convergence curve of MPRR fuel assembly.

# 4. Results and Discussion

The thermo-mechanical fluid–structure interaction (FSI) simulation analysis focused on key performance indicators such as structural deformation, von Mises stress, strain distribution, total elastic strain energy, and velocity streamlines. A comparative validation was performed to identify the solver specific inconsistency and their physical indications.

## 4.1 Structural Deformation

Both Fluent and CFX calculated similar patterns of deformation centered at the mid-span locations of the fuel plates where fluid excitation loads were maximum. The Fluent's peak deformation is slightly higher than that of CFX due to differences in pressure interpolation on the fluid structure boundary. From Fig 9, the maximum deformation for CFX is 0.029268 µm and for Fluent is 0.030156 µm.

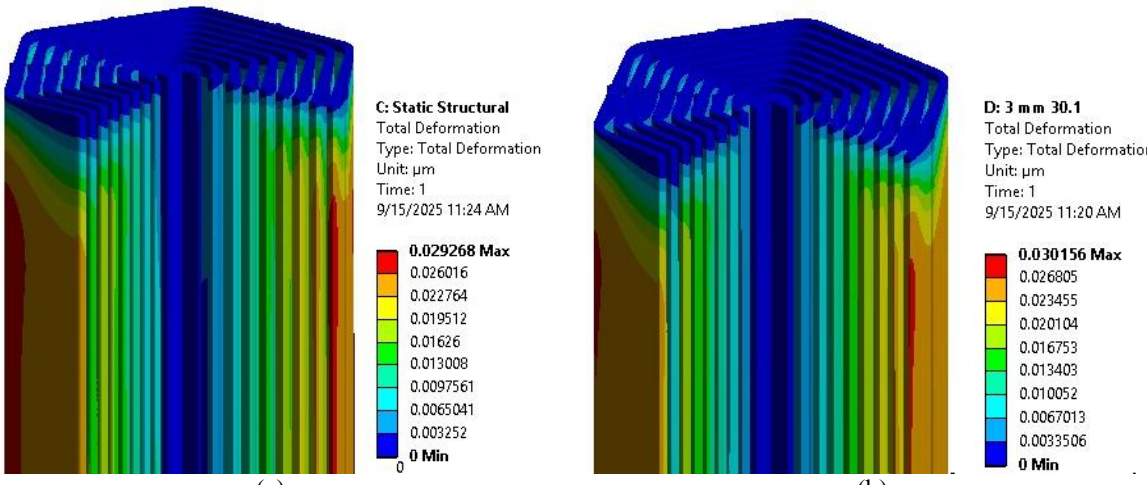


(a) (b)

Figure 9. Structural deformation (a) CFX (b) Fluent.

## 4.2 Stress Distribution

The Von Mises stress contours showed that Fluent gave a smoother stress contour than CFX. From Fig 10, the CFX stress distribution value is 0.46472 MPa that is closer to the Fluent stress distribution value which is 0.46545 MPa

.

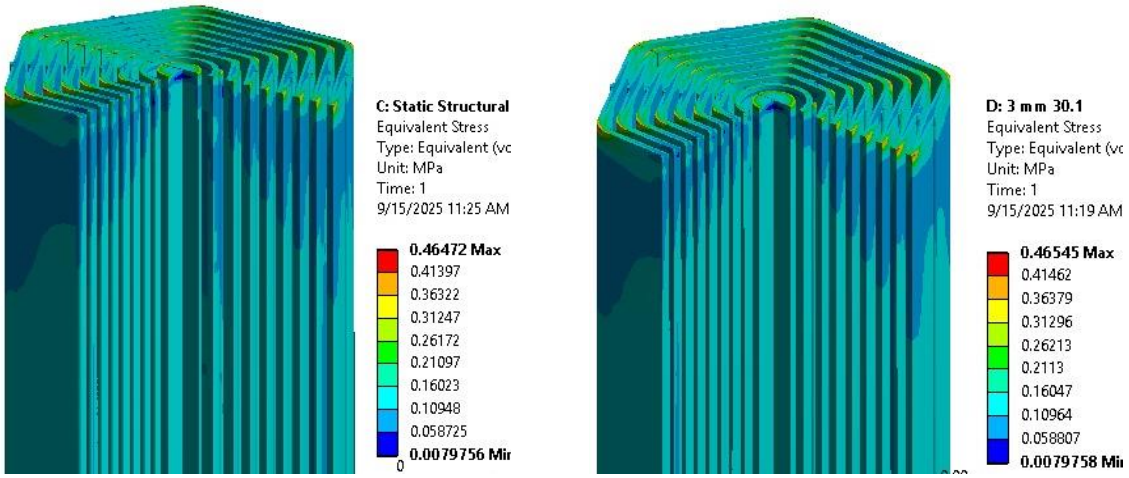


(a) (b)

Figure 10. Stress Distribution (a) CFX (b) Fluent.

lower peak strains. From Fig 11, the CFX strain distribution value is $2.3248 \times 10^{-6}$ µm/ µm that is closer to the Fluent stress distribution value which is $2.3285 \times 10^{-6}$ µm/ µm.

## 4.3 Strain Distribution

Elastic strain was strongly correlated with the displacement profile, with Fluent again showing slightly

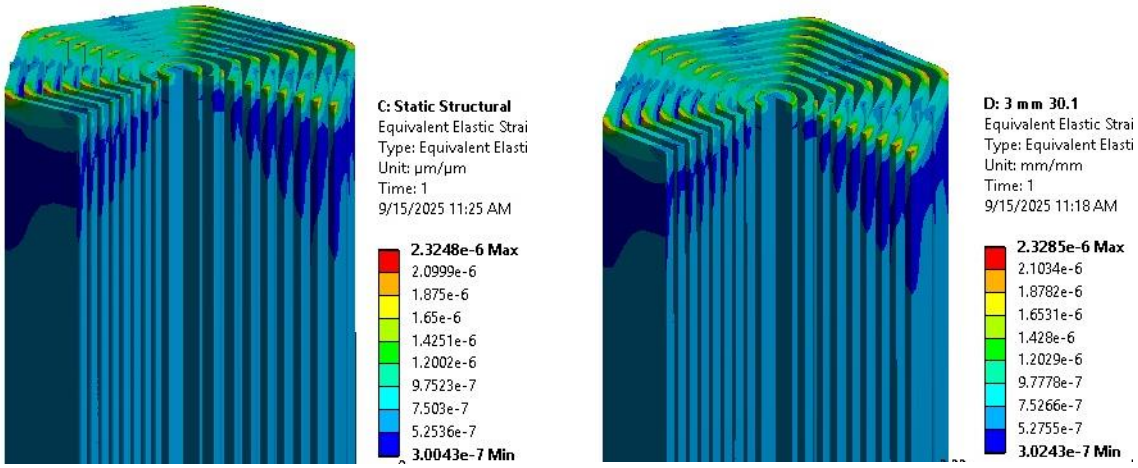


(a) (b)

Figure 11. Strain Distribution (a) CFX (b) Fluent.

## 4.4 Strain Energy

The total strain energy stored in the fuel assembly was extracted to quantify the structural response. The calculated strain energy from Fig 12 for Fluent is 2940.4 pJ and CFX is 2941.5 pJ. The agreement between Fluent and CFX shows a validated result of the analysis.

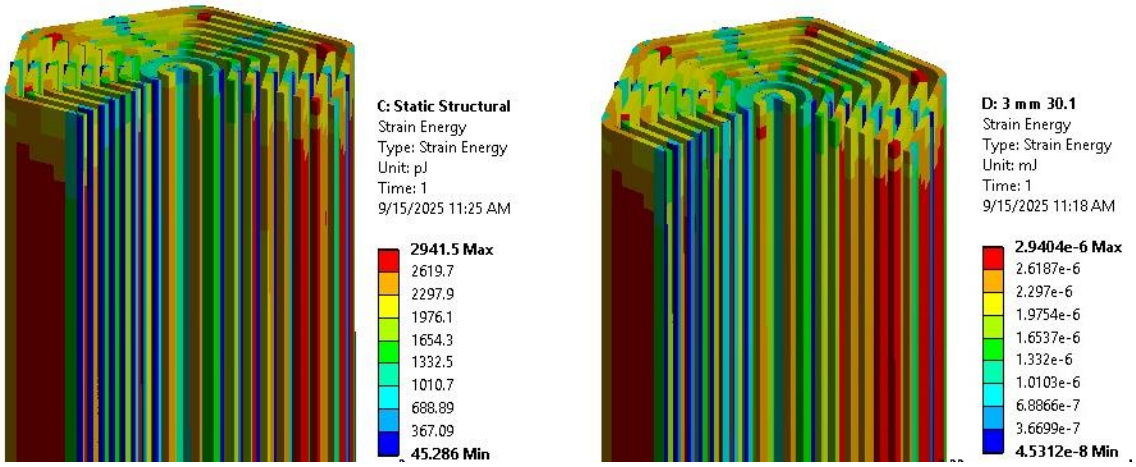


(a) (b)

Figure 12. Strain Energy (a) CFX (b) Fluent.

## 4.5 Velocity Streamlines

A critical comparison was carried out on the velocity streamlines predicted by both solvers. Fluent captured finer-scale vortical structures and localized flow separations near the fuel plate boundaries. In contrast, CFX produced smoother velocity streamlines with less localized fluctuation, aligning with its finite-element based discretization so that they show similar velocity streamlines as mentioned in Fig 13.

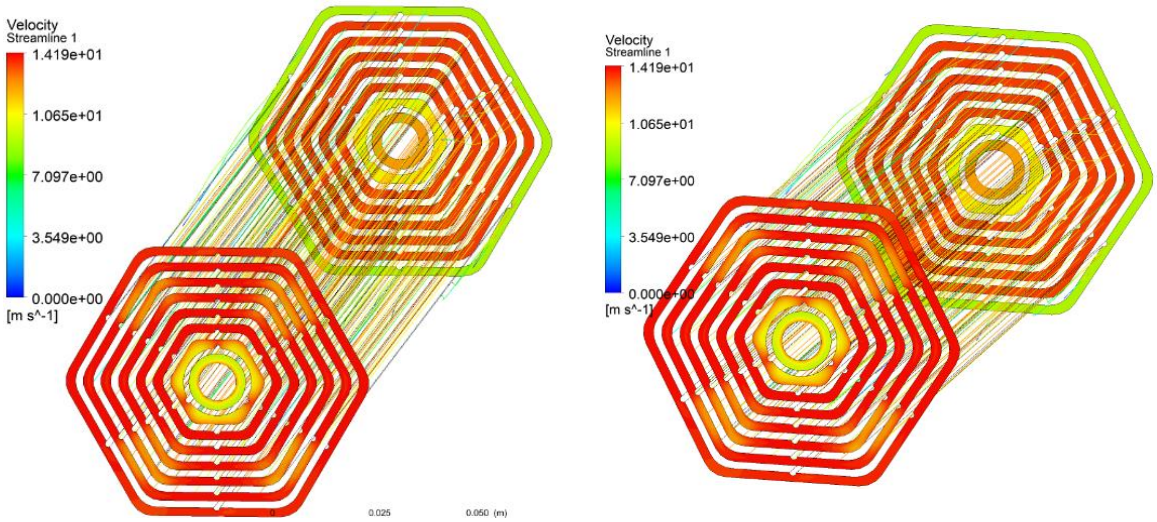


(a) (b)

Figure 13. Velocity Streamlines (a) CFX (b) Fluent.

## 4.6 Inlet Pressure

Figure 14 illustrates the inlet pressure distribution obtained from ANSYS CFX and Fluent. Both solvers predict a nearly uniform pressure field at the inlet, with only slight differences noticeable near the center region. The pressure contours exhibit a smooth and symmetric pattern, confirming that the coolant flow enters the fuel assembly uniformly, which is essential for avoiding localized flow instabilities. The close agreement between the two solvers enhances confidence in the FSI modeling setup, indicating that the inlet boundary conditions are well-defined and that both solvers capture the flow behavior consistently. This uniform pressure distribution ensures an even mass flow rate across all channels, which is crucial for achieving balanced cooling of the fuel rods.

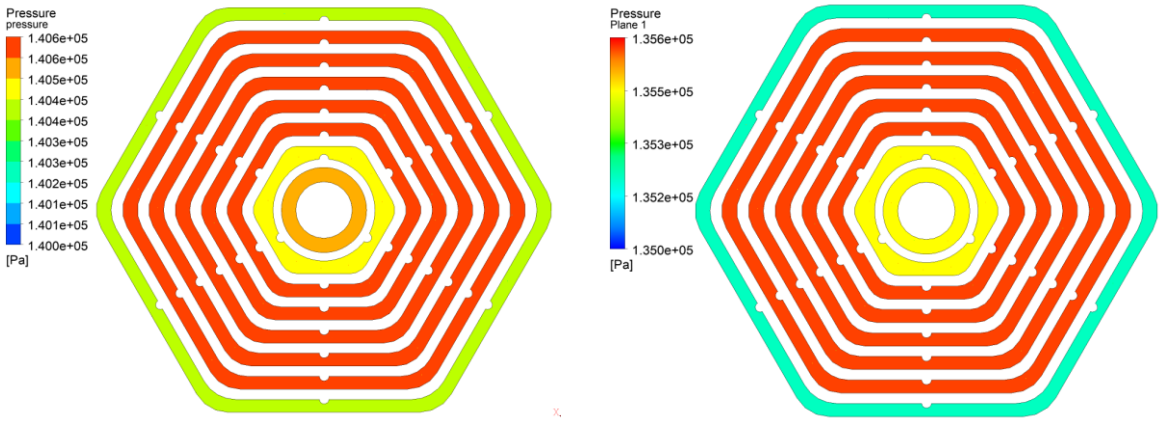


(a) (b)

**FIGURE 14.** Inlet Pressure Contouur (a) CFX (b) Fluent.

## 4.7 Outlet Temperature

Figure 15 shows the outlet temperature distribution predicted by CFX and Fluent. In both cases, the temperature is highest near the central region of the fuel assembly, where power generation is more intense, and gradually decreases toward the outer region, forming a well-defined radial gradient. The nearly identical temperature contours from both solvers indicate strong agreement in capturing heat transfer and coolant temperature rise through the assembly. This consistency validates the thermal-hydraulic model and ensures that the outlet temperature data obtained from Fluent can be reliably applied as a thermal load in subsequent structural analysis. The predicted temperature range also confirms that the fuel assembly operates within safe thermal limits, maintaining effective cooling and minimizing thermal stresses.

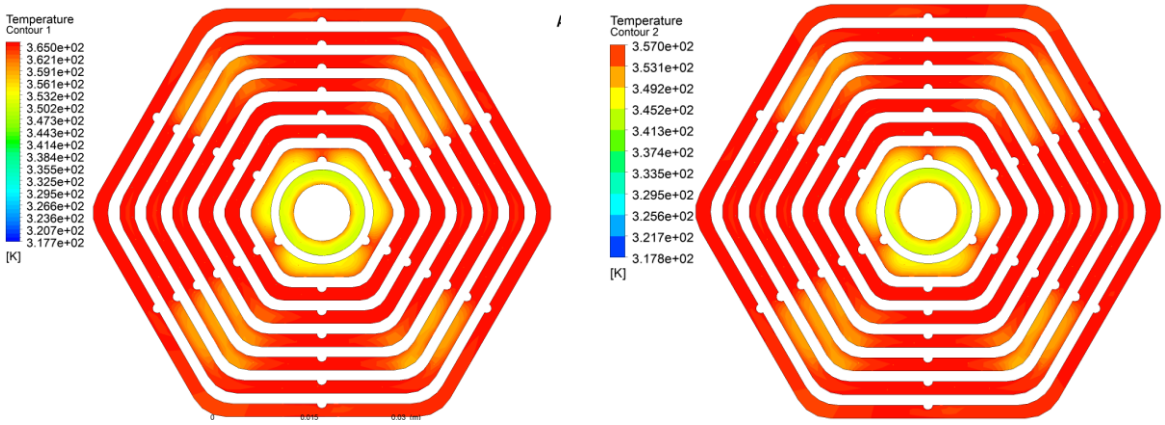


(a) (b)

Figure 15. Outlet Temperature Contouur (a) CFX (b) Fluent.

## 4.8 Velocity Vector Streamlines

The velocity streamline plot shows coolant flowing smoothly through the fuel plate channels, where higher velocities concentrated in the narrow gap and lower velocities near the walls. This indicates effective channeling of flow with localized acceleration and boundary layer effects, ensuring proper coolant distribution within the assembly. The maximum velocity from fig 16 is 14.19 m/s.

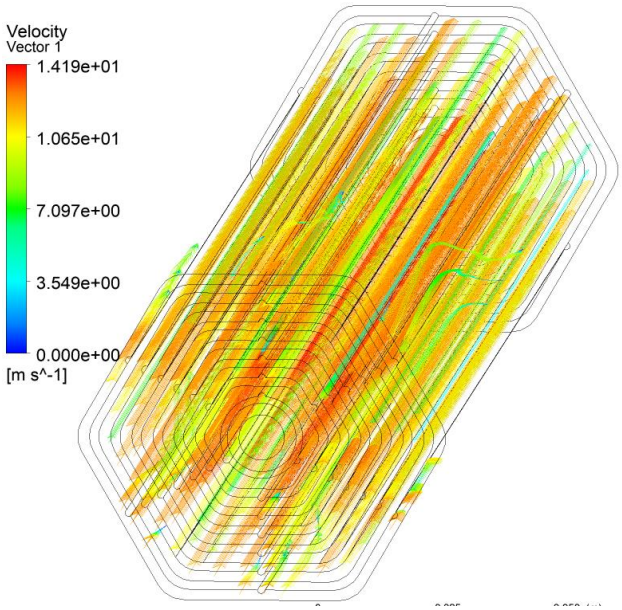


Figure 16. Velocity Vector Streamlines.

The deviation between the inlet velocity (12.26 m/s) and the higher local maximum velocity within the channel (14.19 m/s) occurs due to physical flow development and geometric effects inside the fuel assembly. As the coolant moves through the narrow inter-plate channels, the effective flow area is reduced, and according to the continuity principle Q=A.v, the velocity increases to maintain mass conservation. Additionally, pressure gradients within the channel convert pressure energy into kinetic energy, accelerating the flow and producing higher local velocity than the uniform inlet profile. Local heating of the coolant also lowers fluid density, and for a constant mass flow rate m' =ρAv, this results in a higher volumetric velocity. Furthermore, the fluid-structure interaction causes slight deformation of the fuel plates, reducing channel spacing and intensifying flow acceleration. The developing turbulent profile captured by the standard k–ε model can also predict such velocity peaks due to localized jet-like flow structures and boundary-layer effects. Therefore, the increase to 14.19 m/s is physically realistic and consistent with expected behavior for narrow-gap coolant channels under coupled thermo-mechanical loading, rather than an indication of numerical instability

## 4.9 Temperature Distribution

Figure 17 represents the temperature distribution of the coolant along the fuel height. The horizontal axis indicates the vertical position along the fuel height and vertical axis represents the coolant temperature. The curve shows a gradually increasing temperature profile, indicating that as the coolant flows upward along the fuel channel, its temperature rises due to heat transfer from the fuel rods. The shape of the curve indicates a nonlinear increase, with a steeper gradient near the lower section of the fuel height and a slightly gentler slope toward the upper section, which is typical for convective heat transfer in research reactor cooling systems.

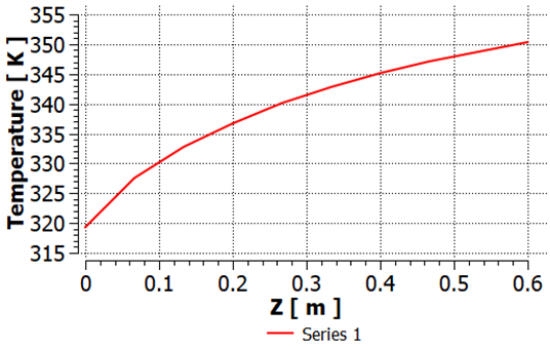


Figure 17. Temperature Distribution along the Fuel Height.

Table 4. Comparative Assessment of Fluent and CFX.

| Parameters | CFX | Fluent | Error |
|---|---|---|---|
| Structural deformation (μm) | 0.029268 | 0.030156 | 2.94% |

| | | | |
|---|---|---|---|
| Stress Distribution (MPa) | 0.46472 | 0.46545 | 0.16% |
| Strain Distribution (µm/ µm) | 2.3248e-6 | 2.3285e-6 | 0.16% |
| Strain Energy (pJ) | 2941.5 | 2940.4 | 0.04% |

Table 4 represents comparative validation of the FSI model that confirms it validated in thermos-mechanical safety analysis.

### 4.10 Sensitivity Test

The sensitivity analysis was conducted to evaluate the impact of ±5% variations in all FSI (Fluent) boundary conditions on the structural and thermal responses of the fuel assembly. The results which show in figs. 18-19 and table 5, indicate a consistent and nearly linear relationship between input perturbations and output responses, demonstrating the robustness of the developed model. A 5% reduction in the input parameters resulted in a measurable decrease in total deformation, equivalent stress, strain distribution, strain energy, and outlet temperature, whereas a 5% increase produced proportionally higher values of these parameters. Among the investigated outputs, equivalent stress and strain energy exhibited the highest sensitivity, implying that mechanical loading and thermal expansion effects are strongly influenced by the applied boundary conditions. In contrast, the inlet pressure distribution remained relatively stable, suggesting that the coolant flow field is less sensitive to minor variations in boundary conditions within the tested range. These findings confirm that the simulation setup captures the physical behavior of the system accurately and identifies critical parameters that should be controlled precisely during reactor operation to maintain structural integrity and thermal safety.

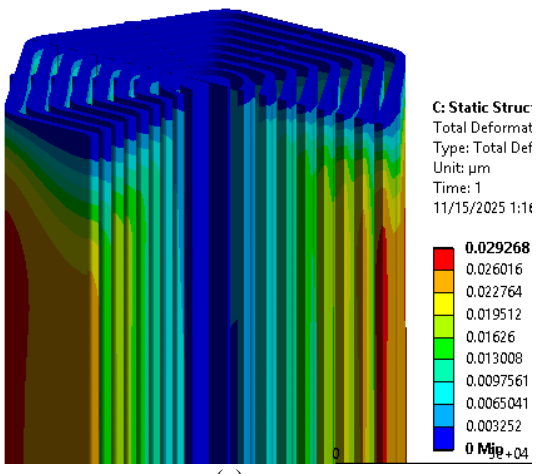


(a)

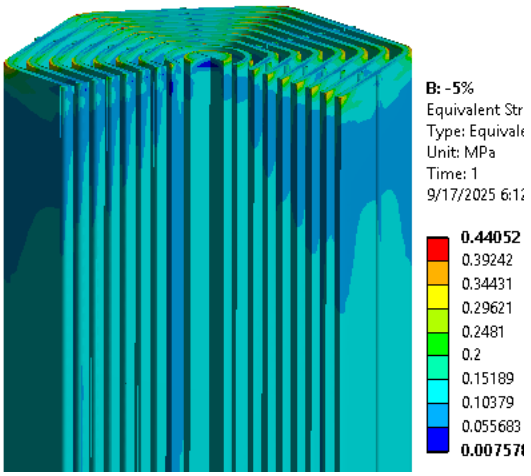


(b)

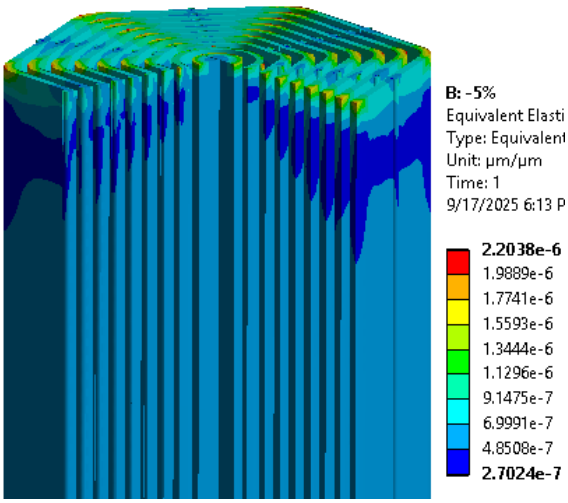


(c)

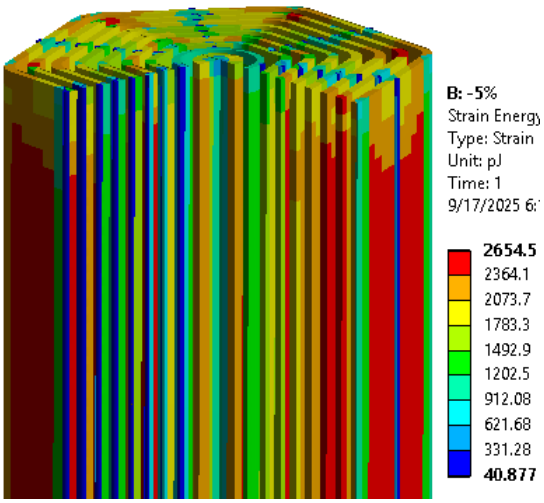


(d)

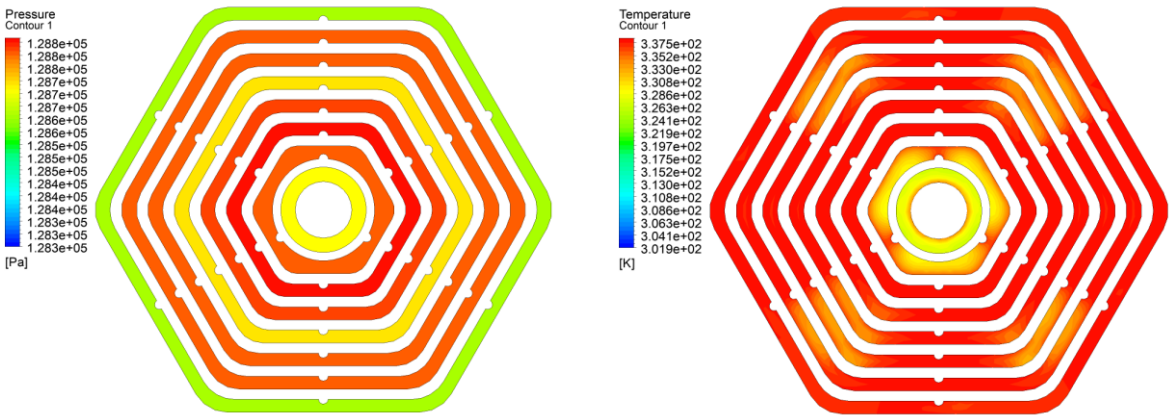


(e) (f)

Figure 18. Comparison of nominal operating condition results with −5% variation in all boundary conditions using FSI (Fluent). (a) Total deformation, (b) Stress, (c) Strain, (d) Strain energy, (e) Inlet pressure, and (f) Outlet temperature.

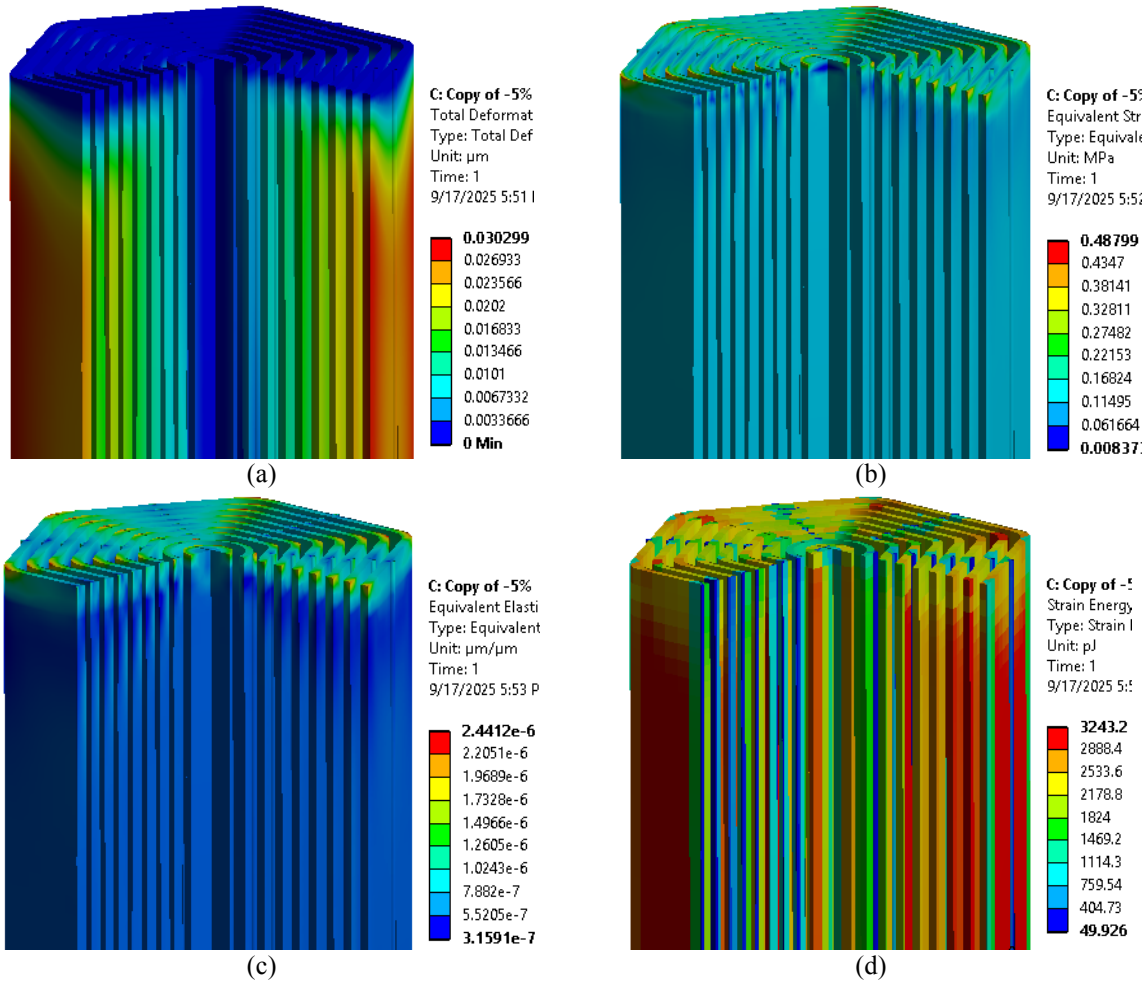


(a) (b)

(c) (d)

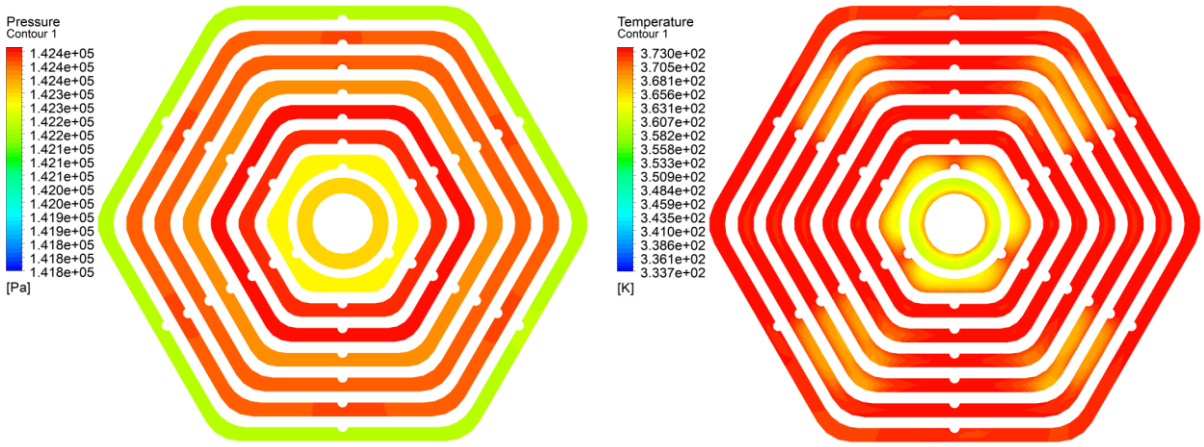


(e) (f)

Figure 19. Comparison of nominal operating condition results with +5% variation in all boundary conditions using FSI (Fluent). (a) Total deformation, (b) Stress, (c) Strain, (d) Strain energy, (e) Inlet pressure, and (f) Outlet temperature.

Table 5. Effect of ±5% Variation in FSI Boundary Conditions on Structural and Thermal Responses

| **Parameters** | Input 5% Decreasing | $D_1$ | Input 5% Increasing | $D_2$ | Original |
|---|---|---|---|---|---|
| Structural deformation (µm) | 0.029268 | -2.94% | 0.030299 | 0.47% | 0.030156 |
| Stress Distribution (MPa) | 0.44052 | -1.16% | 0.48799 | 1.091% | 0.46545 |
| Strain Distribution (µm/ µm) | 2.2038e-6 | -5.36% | 2.4412e-6 | 4.84% | 2.3285e-6 |
| Strain Energy (pJ) | 2654.5 | -9.82% | 3243.2 | 10.18% | 2940.4 |
| Inlet Pressure (MPa) | 0.1288 | -0.09% | 0.1424 | 0.92% | 0.1356 |
| Out temperature (K) | 337.5 | -5.46% | 373 | 4.48% | 357 |

**N.B.** $D_1$ = % change in output for 5% decreasing input and $D_2$ = % change in output for 5% increasing input.

And in case of deviation negative sign is use to indicate decreasing deviation and vice versa.

## 5. Conclusion

The present work demonstrates successful application of FSI in resolving thermo-mechanical response of multipurpose research reactor fuel assemblies. Coupling of CFD and structural solvers through ANSYS Workbench efficiently simulates interaction between the coolant dynamic and structural deformation. The mesh sensitivity study further highlighted the importance of mesh quality. Comparison with validation between Fluent and CFX confirms their concurrence and suitability for nuclear fuel safety simulation.

*References*:

[1] IAEA (International Atomic Energy Agency). (2022). Research Reactors: Purpose and Future. IAEA Technical Report Series No. 982. Vienna: International Atomic Energy Agency.

[2] Zulquarnain, M., Haque, M., Salam, M., Islam, Saha, P., Sarder, M., Haque, A., Soner, M., Uddin, M., Rahman, M., Kamal, I., Islam, M., & Hossain, S. (2009). Experience with the operation, maintenance and utilisation of the 3 MW TRIGA Mark-II research reactor of Bangladesh. International Journal of Nuclear Energy Science and Technology, 4(4), 299. https://doi.org/10.1504/ijnest.2009.028591

[3] Framatome. (2023, March 7). Framatome completes first fuel element for the U.S. TRIGA research reactors. [Press release]. Retrieved from https://www.framatome.com/medias/download/?id=15082&n=framatome-completes-first-fuel-element-for-the-us-triga-research-reactors.

[4] Arinkin, F. M., Shaimerdenov, A. A., Gizatulin, S. K., Dyusambaev, D. S., Koltochnik, S. N., Chakrov, P. V., & Chekushina, L. V. (2017).

[5] Core conversion of VVR-K research reactors. Atomic Energy, 123(1), 17–24. https://doi.org/10.1007/s10512-017-0294-0.

[6] Shanta, S. N. J., & Mollah, A. S. (2025). Structural and thermal analysis of fuel rod of VVER-1200 nuclear reactor using ANSYS software. MIST INTERNATIONAL JOURNAL OF SCIENCE AND TECHNOLOGY, 13, 65–71. https://doi.org/10.47981/j.mijst.13(01)2025.510(65-71

[7] De Vaucorbeil, A., Nguyen, V. P., Sinaie, S., & Wu, J. Y. (2020). Material point method after 25 years: Theory, implementation, and applications. In Advances in applied mechanics (pp. 185–398). https://doi.org/10.1016/bs.aams.2019.11.001

[8] Liu, B., Yan, Q., & Wei, W. (2018). Numerical investigations of the flow induced oscillation of a torque converter. Engineering Applications of Computational Fluid Mechanics, 12(1), 270–281. https://doi.org/10.1080/19942060.2017.1419149

[9] Zahid, M., Mehedi, I., Shiby, S., & Mollah, A. (2024). Thermal hydraulic analysis for different subchannels of generic VVER-1200. International Journal of Nuclear Security, 9(2). https://doi.org/10.7290/ijns09147839

[10] Shaheed, R., Mohammadian, A., & Gildeh, H. K. (2018). A comparison of standard k–ε and realizable k–ε turbulence models in curved and confluent channels. Environmental Fluid Mechanics, 19(2), 543–568. https://doi.org/10.1007/s10652-018-9637-1

[11] Adam, N. M., Attia, O. H., Al-Sulttani, A. O., Mahmood, H. A., As'arry, A., & Rezali, K. a. M. (2020a). Numerical Analysis for Solar Panel Subjected with an External Force to Overcome Adhesive Force in Desert Areas. CFD Letters, 12(9), 60–75. https://doi.org/10.37934/cfdl.12.9.6075

[12] Lee, C., Abe, Y., Kawano, Y., & Yamazaki, T. (2025). Fluid-structure interaction analysis with interface control principle. *arXiv (Cornell University)*. https://doi.org/10.48550/arxiv.2510.17144

[13] Chaudhry, V., Kumar, A., Ingole, S., Balasubramanian, A., & Muktibodh, U. (2014). Thermo-mechanical transient analysis of reactor pressure vessel. Procedia Engineering, 86, 809–817. https://doi.org/10.1016/j.proeng.2014.11.101

[14] Deng, Y., Wu, Y., Zhang, D., Lu, Q., Tian, W., Qiu, S., & Su, G. (2016). Thermal-mechanical coupling behavior analysis on metal-matrix dispersed plate-type fuel. Progress in Nuclear Energy, 95, 8–22. https://doi.org/10.1016/j.pnucene.2016.11.007

**Contribution of Individual Authors to the Creation of a Scientific Article (Ghostwriting Policy)**

The authors equally contributed in the present research, at all stages from the formulation of the problem to the final findings and solution.

**Sources of Funding for Research Presented in a Scientific Article or Scientific Article Itself**

No funding was received for conducting this study.

**Conflict of Interest**

The authors have no conflicts of interest to declare that are relevant to the content of this article.